Protein Science (1995), *4*:1262–1271. Cambridge University Press. Printed in the USA.

High-resolution structures of adenylate kinase from yeast ligated with inhibitor Ap_5A, showing the pathway of phosphoryl transfer

U. ABELE AND G.E. SCHULZ

Institut für Organische Chemie und Biochemie, Albert-Ludwigs-Universität, 79104 Freiburg im Breisgau, Germany

(RECEIVED December 30, 1994; ACCEPTED March 24, 1995)

Abstract

The structure of adenylate kinase from yeast ligated with the two-substrate-mimicking inhibitor Ap_5A and Mg^{2+} has been refined to 1.96 Å resolution. In addition, the refined structure of the same complex with a bound imidazole molecule replacing Mg^{2+} has been determined at 1.63 Å. These structures indicate that replacing Mg^{2+} by imidazole disturbs the water structure and thus the complex. A comparison with the G-proteins shows that Mg^{2+} is exactly at the same position with respect to the phosphates. However, although the Mg^{2+} ligand sphere of the G-proteins is a regular octahedron containing peptide ligands, the reported adenylate kinase has no such ligands and an open octahedron leaving space for the Mg^{2+} to accompany the transferred phosphoryl group. A superposition of the known crystalline and therefore perturbed phosphoryl transfer geometries in the adenylate kinases demonstrates that all of them are close to the start of the forward reaction with bound ATP and AMP. Averaging all observed perturbed structures gives rise to a close approximation of the transition state, indicating in general how to establish an elusive transition state geometry. The average shows that the in-line phosphoryl transfer is associative, because there is no space for a dissociative metaphosphate intermediate. As a side result, the secondary dipole interaction in the α-helices of both protein structures has been quantified.

Keywords: adenylate kinase; phosphoryl transfer; substrate binding; X-ray structure

Adenylate kinases catalyze the transfer of a phosphoryl group according to: $ATP \cdot Mg^{2+} + AMP \rightleftharpoons Mg^{2+} + ADP + ADP$. They are ubiquitous; several amino acid sequences are known and can be related to each other (Schulz, 1987). Adenylate kinases are monomeric and have been subdivided into small and large variants with M_r of about 21,000 and 24,000, respectively. Moreover, adenylate kinases have a significant relationship with a series of other nucleotide binding proteins, in particular G-proteins (Pai et al., 1990; Noel et al., 1993; Coleman et al., 1994), showing a particularly high similarity in the central part of the sheet that contains the giant anion hole with the fingerprint sequence -Gly-x-x-Gly-x-Gly-Lys- (Schulz, 1992). Refined high-resolution structures had been reported for adenylate kinases from pig muscle cytosol (AK1; Dreusicke et al., 1988), from the bovine mitochondrial matrix (AK3; Diederichs & Schulz, 1991), and from *Escherichia coli* (AK_{eco}; Müller & Schulz, 1992; Berry et al., 1994); a low-resolution structure is known for the enzyme from carp (Reuner et al., 1988).

Here we report two refined structures of the adenylate kinase from yeast, which is a large variant and consists of 220 amino acid residues with an M_r of 24,077 (see Kinemages 1 and 2; Tomasselli et al., 1986; Magdolen et al., 1987; Proba et al., 1987). In one crystal form that has been elucidated at 1.96 Å resolution, AK_{yst} is ligated with the two-substrate-mimicking inhibitor Ap_5A and Mg^{2+}. This structure had been reported at medium resolution with some insufficiently defined loops by Egner et al. (1987). In the other crystal form that has been determined at 1.63 Å resolution, AK_{yst} is ligated with Ap_5A and an imidazole molecule at the Mg^{2+} site. The structures improve our knowledge of the catalytic mechanism.

Reprint requests to: Georg E. Schulz, Institut für Organische Chemie und Biochemie, Albert-Ludwigs-Universität, Albertstrasse 21, 79104 Freiburg im Breisgau, Germany; e-mail: schulz@bio2.chemie.uni-freiburg.de.

Abbreviations: AK_{eco}, adenylate kinase from *Escherichia coli*; AK_{yst}, adenylate kinase from yeast; Ap_5A, P^1,P^5-bis(5′-adenosyl)pentaphosphate; *B*-factor, crystallographic temperature factor; Im, imidazole; Im-structure, crystalline complex AK_{yst}:Ap_5A:Im; Mg-structure, crystalline complex AK_{yst}:Ap_5A:Mg; NMP, nucleoside monophosphate; PEG, polyethyleneglycol; σ, standard deviation.

Results and discussion

Model accuracies

The main parameters for the two refined structure models are listed in Table 1. In both models the polypeptide chain consists

Table 1. *Crystallographic data and qualities of the resulting models*

	AK_{yst}:Ap_5A:Im	AK_{yst}:Ap_5A:Mg
Resolution range (Å)	10–1.63	10–1.96
Number of unique reflections	25,745	15,477
Completeness (%)	97.4	99.2
Crystallographic *R*-factor (%)	19.4	17.6
RMS bond length deviations (Å)	0.007	0.010
RMS bond angle deviations (deg)	1.3	1.4
Coordinate error estimate[a] (Å)	0.22	0.22
Coordinate error estimate[b] (Å)	0.24	0.26
Real space correlation coefficient[c]	0.89	0.90
Number of modeled atoms		
Polypeptide	1,675	1,675
Ap_5A	57	57
Ligand	5	1
Solvent	131	153
Average *B*-factor		
Main chain	30	27
Ap_5A	15	14
Adenosine at ATP site	18	17
Adenosine at AMP site	12	12
Ligand	29	15
Solvent	45	40

[a] According to Luzzati (1952).
[b] Derived from σ_A-plots following Read (1986).
[c] Polypeptide average according to Jones et al. (1991).

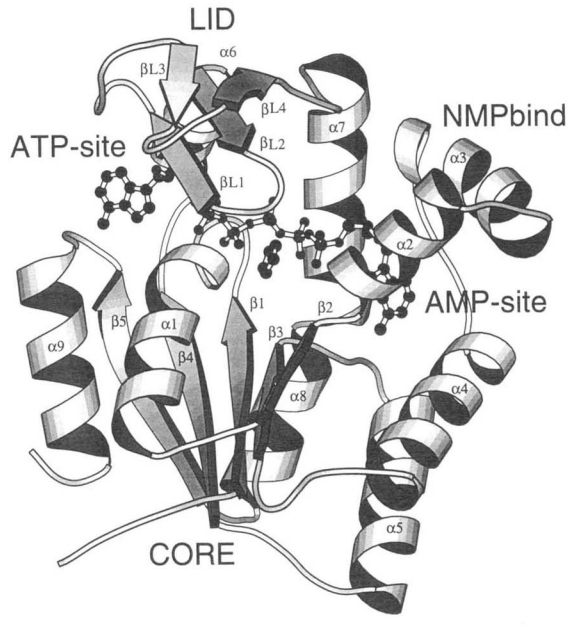

Fig. 1. Ribbon-plot of AK_{yst} with inhibitor Ap_5A and imidazole drawn with MOLSCRIPT (Kraulis, 1991). The sites of the substrates ATP and AMP are labeled. The domains CORE, LID, and NMPbind are indicated. See Figure 3 for names of secondary structures.

of residues 3–220; both N-termini are disordered. The coordinate errors are about 0.24 Å (Table 1), which is confirmed by the C^α distance plot (see below Fig. 2A) if the mobile domains LID and NMPbind are disregarded. The correlation coefficients between density and model (Jones et al., 1991) were about 90% for both models and thus satisfactory (Table 1).

As another accuracy check, we inspected the (χ_1, χ_2) scatter plots for the 21 Leu and the 15 Ile residues and found them concentrated at the usual staggered positions. After excluding Leu 9, which is affected by Im binding, the average deviations from stagger were 8° for the Im-structure and 9° for the Mg-structure.

Chain fold

Like the other adenylate kinases, AK_{yst} consists of a five-stranded parallel β-sheet with surrounding α-helices. The chain folds of the two reported structures are similar enough to be both well described by the ribbon plot in Figure 1 (see also Kinemage 1). Both structures are likely to deviate from the natural conformation around the additional phosphate P_4 of the inhibitor Ap_5A. The Im-structure has a further perturbation because it has the bulky Im ring at the position of the small Mg^{2+} ion. The polypeptide had been subdivided into three domains: CORE (here residues 5–33, 64–130, and 169–218) comprises the central parallel β-sheet and adjacent helices, NMPbind (34–63) encloses the bound AMP, and LID (131–168) covers the bound ATP and the phosphoryl transfer region (Schulz et al., 1990).

In order to elucidate the differences between the two structures, we superimposed them on their C^α atoms of CORE, which is the central rigid part. The best superposition was achieved after a relative 1.5° rotation of the CORE domains, indicating a slight packing rearrangement in the crystals. The superimposed CORE domains have an RMS C^α deviation of only 0.21 Å (Fig. 2A), which is below the general error estimate. With this superposition, the NMPbind domains show an RMS C^α deviation of 0.30 Å, indicating a minor motion relative to CORE. The LID domain movement is larger as the corresponding RMS C^α deviation amounts to 1.25 Å. However, a separate superposition of the LID domains reduces this deviation to 0.45 Å after a relative rotation of 5°. LID rotations of similar magnitude had been observed with AK_{eco} after introducing bulky side chains into the glycine-rich loop near the Mg^{2+} site (Müller & Schulz, 1993). The relatively large residual C^α deviation of 0.45 Å in the LID comparison is probably caused by the high mobility of this domain indicated by high *B*-factors (Fig. 2B).

Chain conformations

A Ramachandran plot of the higher resolution structure AK_{yst}:Ap_5A:Im shows none of the residues in a forbidden region. There are two non-glycine residues with well-defined electron densities, His 29 and Met 153, in the left-handed α-helical region around (+50°, +30°). In several other adenylate kinases, the equivalent residues are glycines. A manual secondary structure assignment is given in Figure 3 together with the amino acid sequence. Noticeable are the two 3_{10}-helices around residues 82 and 185.

The side-chain dihedral angles χ_1 of the Im-structure are distributed as usual (Dunbrack & Karplus, 1993) over the staggered positions g^+, t, and g^-. There are five residues close to eclipsed positions: Leu 9 ($\chi_1 = 222°$) is affected by the bound Im; Ser 64

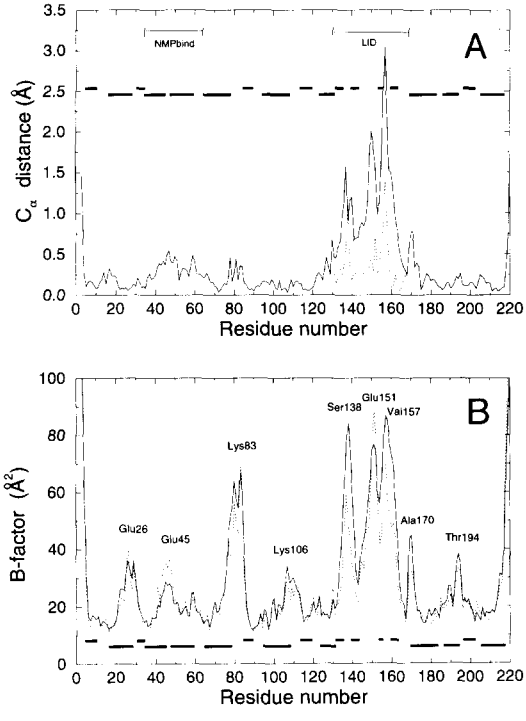

Fig. 2. Main-chain deviations. Secondary structures are given as black bars with β-strands slightly above α-helices. **A:** Residual C^α distance between AK_{yst}:Ap_5A:Im and AK_{yst}:Ap_5A:Mg after best superposition of the CORE domains (C^α atoms 5–33, 64–130, and 169–218). The dotted line corresponds to a superposition of the LID domains (C^α atoms 131–168). **B:** Main-chain *B*-factors of AK_{yst}:Ap_5A:Im (solid line) and AK_{yst}:Ap_5A:Mg (broken line). In the final refinement rounds, the RMS *B*-factor deviations were 1.5 Å for neighboring atoms and 2 $Å^2$ for two atoms connected via a third one. Relative maxima are labeled.

($\chi_1 = 129°$) forms hydrogen bonds to Asp 65-N as well as Ile 67-N; Arg 165 ($\chi_1 = 252°$) is pushed away by the additional phosphate P_4 of Ap_5A; and Glu 185 ($\chi_1 = 220°$) and Lys 216 ($\chi_1 = 260°$) form salt bridges to His 181 and Asp 212, respectively. Angle χ_2 was only scrutinized for Leu and Ile as described above. Altogether, the model behaves properly.

The Mg-structure AK_{yst}:Ap_5A:Mg has a Ramachandran plot very similar to the Im-structure; the RMS difference is 9° in each of the angles ϕ and ψ. The secondary structure assignments are identical (Fig. 3). The χ_1 distributions correspond to each other, except for Leu 9, which is here staggered in g^+. During manual α-helix assignment, we realized that the amides have a second hydrogen bond acceptor atom at distances around 3.4 Å. Although this secondary acceptor is much worse positioned than the primary acceptor, it is still likely to affect the primary hydrogen bond. A scatter plot (Fig. 4) shows that the lengths of primary and secondary bonds are coupled, there is a continuous transition from α-helix (upper left) to 3_{10}-helix (lower right). This secondary interaction should be considered when discussing hydrogen bond energies in α-helices and β-sheets. The bonds between β-strands are on average about 0.1 Å shorter (Baker & Hubbard, 1984), but not necessarily stronger as they lack the secondary interaction.

Chain mobility and solvent

Atom mobilities are described by crystallographic temperature factors, the distributions of which agree well for the two reported structures (Fig. 2B). The most rigid part is the CORE domain and in particular the five central β-strands. The highest *B*-factors occur at the chain termini and in the LID domain, which explains the chain fitting problems of Egner et al. (1987) in this domain. The second largest peak is around residue 80, where an α-helix tapers out to a 3_{10}-helix.

It should be noted that the mobility peaks at the chain termini as well as at positions 26, 45, 83, 106, and 194 (Fig. 2B) are all close together at one side of the enzyme, i.e., at the bottom of Figure 1 and Kinemage 1. It is conceivable that this surface is used for an association with another component of the cell. Such an association would occur far away from the active center and would be unlikely to interfere with catalysis.

The Im-structure contains 131 water molecules sorted according to electron density (numbers start at 501). They constitute 16% of all crystal water. The Mg-structure contains 22 more water molecules (Table 1). Part of this difference is caused by the lack of visible water at the LID domain of the Im-structure, which could be a consequence of its higher mobility. The largest mobility increase occurs at Gly 139-O (data not shown), which is well connected via water molecules around Ap_5A in the Mg-structure, but only loosely bound in the Im-structure (see

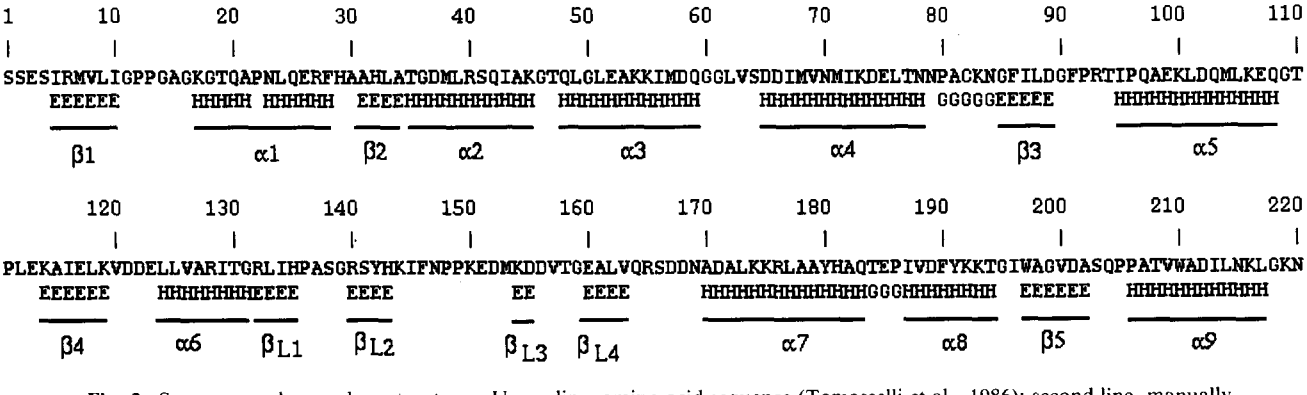

Fig. 3. Sequence and secondary structures. Upper line, amino acid sequence (Tomasselli et al., 1986); second line, manually assigned secondary structures (E, β-sheet; H, α-helix; G, 3_{10}-helix) for both structures; third line, assigned names of β-strands and α-helices. β-Strands of LID are named separately because this domain is not present in small variants.

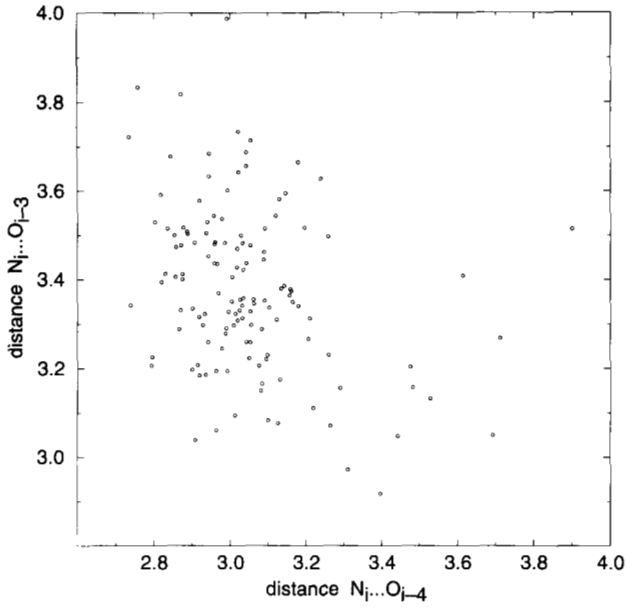

Fig. 4. Relation between the lengths of primary and secondary hydrogen bonds in α-helices as referred to the donor amide at position *i*. The plot contains all α-helical H-bonds (Fig. 3) from both reported structures. Average angles N_i-$\hat{H}_i \cdots O_{i-4}$ and N_i-$\hat{H}_i \cdots O_{i-3}$ are 161° and 111°, respectively.

below, Fig. 6). Apparently, the bulky imidazole disturbs the natural water structure.

In both structures, we find that 15% of all assigned water molecules have *B*-factors below the main-chain average and densities above 3σ, such that they can be considered as integral parts of the protein (Karplus & Schulz, 1987).

Crystal packing

Both structures belong to space group P1, with closely resembling molecular packings that are depicted in Figure 5 and described in Table 2. The major contacts I, II, and III have similar sizes and they connect the molecules along the unit cell axes *a*, *b*, and *c*, respectively. This uniform contact distribution agrees well with the globular habit of the crystals. In addition, there are two small "diagonal" contacts, IV and V. Relating the crystal contact areas of a given molecule to its total solvent-accessible surface area, we find 2,690 Å^2/10,250 Å^2 = 26% for the Im-structure and 2,480 Å^2/9,910 Å^2 = 25% for the Mg-structure, resembling those of other adenylate kinases.

Binding of Ap_5A

The inhibitor Ap_5A can be considered as an ATP molecule coupled to an AMP via the additional phosphate P_4. Because Ap_5A is a covalently symmetrical molecule, its binding mode fails to distinguish between the ATP and the AMP site. The site assignment (Fig. 1; Kinemage 1) was done with homologous structures containing only one nucleotide (Diederichs & Schulz, 1990; Stehle & Schulz, 1990) and with mutation data (Tsai & Yan, 1991); it was recently confirmed by an adenylate kinase structure containing an ATP analog and AMP (Berry et al., 1994).

The inhibitor binds tightly as demonstrated by its low *B*-factors (Table 1). The polar contacts between Ap_5A and the polypeptide are listed in Table 3. The binding mode is similar to Ap_5A bound to AK_{eco} (Müller & Schulz, 1992). Only the additional

Table 2. *Crystal contacts*

Contacts	Buried surface[a] (Å^2)	Residues involved[b]	Polar contacts[c]	Distance[a] (Å)
I[d]	340 (365)	a-b_1	Lys 45-NZ···Glu 185-OE1	3.22 (3.75)
	340 (365)	b-a_2		
II	430 (390)	c-d_3	Glu 52-OE1···Ala 207-N	2.96 (2.91)
			Glu 52-OE1···Thr 208-N	– (3.33)
			Glu 52-OE1···Thr 208-OG1	– (2.69)
			Asn 70-ND2···Asn 229-OD1	– (3.16)
	430 (390)	d-c_4		
III	365 (325)	e-f_5	Glu 123-O···Lys 106-NZ	– (3.10)
			Thr 130-OG1···Glu 107-O	3.46 (2.81)
	365 (325)	f-e_6		
IV	115 (65)	g-h_7		
	115 (65)	h-g_8		
V	95 (95)	i-j_9		
	95 (95)	j-i_{10}		

[a] Calculation for AK_{yst}:Ap_5A:Im using XPLOR (probe radius of 1.4 Å); values for AK_{yst}:Ap_5A:Mg are in parentheses.

[b] Contacting molecules 1–10 are related by the following 10 translations: 1 = (1,0,0); 2 = (−1,0,0); 3 = (0,1,0); 4 = (0,−1,0); 5 = (0,0,1); 6 = (0,0,−1); 7 = (1,0,1); 8 = (−1,0,−1); 9 = (1,−1,0); 10 = (−1,1,0). Using a 4.5-Å distance criterion the contacting residues in the Im-structure are: *a* = (44–45,78); *b* = (122,181,185,192–193); *c* = (48–49,52,64,66–67,70); *d* = (147,205–208,211–212,215,220); *e* = (123,126–127,130,144–145,170); *f* = (83,106–110); *g* = (153); *h* = (193,195); *i* = (151); *j* = (175). In the Mg-structure, the contacts contain the following additional residues: *a*(80,160), *b*(124,189,197), *c*(73), *g*(154), *h*(194).

[c] Using a 3.5-Å distance criterion.

[d] This contact is divided into two areas.

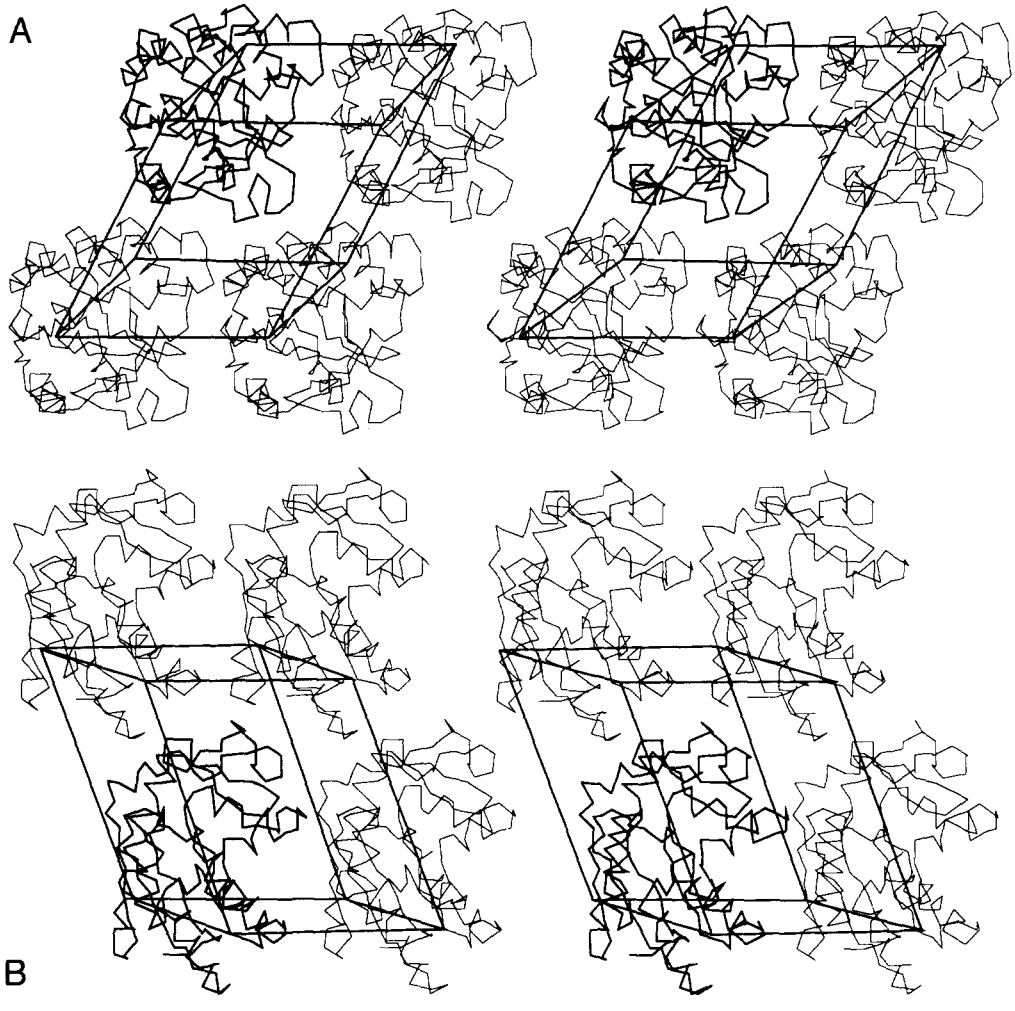

Fig. 5. Crystal packing in AK_{yst}:Ap_5A:Im. AK_{yst} is given as a C^{α} chain fold; Ap_5A is omitted for clarity. **A:** **a**–*b* plane, *a* is horizontal. **B:** **a**–*c* plane.

phosphate P_4 varies, indicating that the yeast enzyme found an alternative way for accommodating this intruder. The Ap_5A differences between the Im- and Mg-structures are minor; they appear to be explained by the size difference between Im and Mg^{2+}.

The adenosine *B*-factors in Table 1 show that the ATP site is less well defined than the AMP site. The same information can be deduced from Table 3, which shows only one hydrogen bond to the ATP-adenosine but five to the other. Even the sketch in Figure 1 points out that the ATP-adenosine is rather exposed to the solvent, whereas the AMP-adenosine is completely buried. We therefore conclude that the AMP site is a normal deep pocket formed after an appreciable induced-fit movement of domain NMPbind (Schulz et al., 1990) in agreement with the observed high specificity for this substrate. In contrast, ATP is predominantly fixed at its β-phosphate in the giant anion hole (Dreusicke & Schulz, 1986).

Imidazole binds with its N1 atom at the position of the Mg^{2+} ion (Table 3). Its N3 atom forms a hydrogen bond to the highly conserved Asp 89, which normally holds two water ligands of Mg^{2+}. The binding arrangements of Im and Mg^{2+} are depicted in Figure 6. Mg^{2+} is identified by the correspondence of its *B*-factor with those of the neighboring phosphates. Mg^{2+} binds between phosphates P_2 and P_3 (β- and γ-phosphates of ATP). A similar binding position had been reported by Egner et al. (1987), who identified the approximate Mg^{2+} location of this site at low resolution by soaking with 10 mM $MnCl_2$.

Figure 6A and Kinemage 2 show an extensive water cluster in the active center in the Mg-structure that connects to the LID and NMPbind domains via water molecules 551 and 603, respectively. The intruder Im shown in Figure 6B and Kinemage 2 replaces three and displaces one of these water molecules. A superposition of the active centers is given in Figure 7 and Kinemage 2, showing an appreciable displacement of the LID domain in agreement with Figure 2A. The additional fourth phosphate undergoes the largest change of the phosphate chain; apparently it is moved around because it has no established binding site.

Phosphoryl transfer

Because one cannot stabilize an active enzyme:substrate complex, all crystal structure data refer at best to states that are close to this natural complex. For the adenylate kinase family, we

Table 3. *Hydrogen bonds between Ap_5A and polypeptide*

Ap_5A[a]	Contacting atom[b]	D···A[c] (Å)	Ap_5A[a]	Contacting atom[b]	D···A[c] (Å)
N1A	Arg 128-NH1	3.42(3.57)	OP3S	Gly 14-N	3.70(3.50)
N10A	Gln 204-O	2.75(2.71)		Arg 132-NH1	2.86(2.71)
OP1R	Gly 18-N	3.32(3.31)		Arg 132-NH2	3.42(3.23)
	Thr 19-N	2.99(3.01)		Arg 176-NH1	2.76(2.77)
	Thr 19-OG1	2.75(2.70)	OP4R	Lys 17-NZ	2.73(2.92)
OP1S	Arg 132-NH2	2.91(2.93)		Arg 93-NH1	3.03(3.05)
	Ser 141-OG	3.10(2.89)		Arg 93-NH2	2.98(2.89)
O12	Arg 132-NH2	3.43(3.47)	OP4S	Arg 176-NH1	2.95(3.02)
OP2R	Ala 15-N	3.22(3.38)	OP5S	Arg 40-NH1	2.89(2.93)
	Gly 16-N	2.80(2.86)		Arg 40-NH2	3.07(3.05)
	Lys 17-N	2.91(2.94)		Arg 165-NH1	3.43(3.31)
OP2S	Gly 18-N	2.95(2.91)		Arg 165-NH2	3.42(3.28)
	Im-N1	2.72	OP5R	Arg 93-NH1	2.85(2.74)
O23	Gly 14-N	3.14(3.18)	O5RB	Arg 93-NH1	3.59(3.48)
OP3R	Arg 132-NH2	3.08(3.09)	N1B	Gln 97-NE2	3.04(2.96)
	Arg 165-NH2	2.91(2.88)	N3B	Val 63-N	3.17(3.09)
	Im-N1	2.69	N10B	Gly 90-O	2.98(2.94)
				Gln 97-OE1	3.13(3.06)

[a] The letters A and B at the adenosine atoms refer to the ATP and AMP sites, respectively. Phosphates are numbered 1–5, starting from the ATP site. Values for the Im-structure are given directly; those for the Mg-structure are in parentheses.

[b] For AK_{yst}:Ap_5A:Im there are 7 contacting water molecules (3.5 Å criterion), whereas there are 11 contacting water molecules in AK_{yst}:Ap_5A:Mg.

[c] Hydrogen bonds are defined by donor···acceptor distances below 3.5 Å and D-Ĥ···A angles above 90°. Violations of these criteria are marked by underscores.

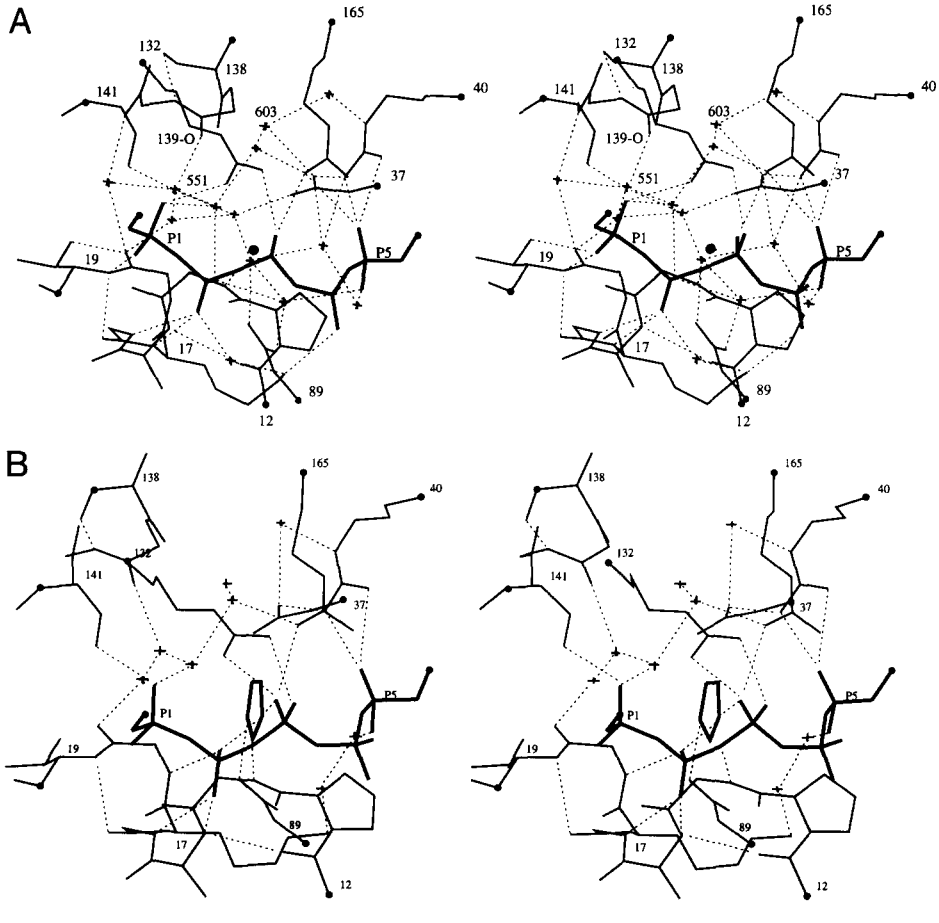

Fig. 6. Binding of Im and Mg^{2+} in AK_{yst} ligated with Ap_5A. Most residues and two water molecules are labeled. Chain cuts are marked by dots. **A:** Position of Mg^{2+} (dot) in an extended water cluster. Detailed environment of Mg^{2+} is shown in Figures 8B and 9. **B:** Binding of Im as suspended between the third phosphate and Asp 89. Imidazole disturbs appreciably the water network at the active center.

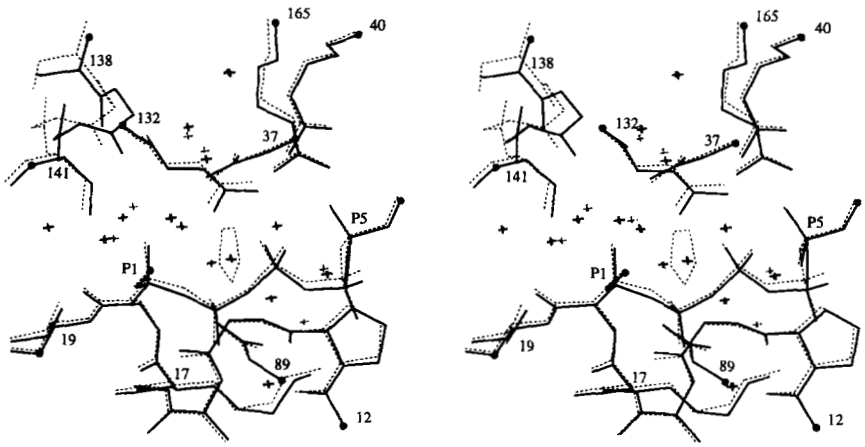

Fig. 7. Superposition of the phosphates, the active center water molecules, and the surrounding polypeptide residues in AK_{yst}:Ap_5A:Mg (solid lines) and AK_{yst}:Ap_5A:Im (dotted lines). The superposition is based on the CORE domains (defined e.g., in Fig. 2). The uppermost water molecules near residue 165 overlap almost completely. The Mg^{2+} ion is close to N1 of Im, which is the ring atom nearest to phosphate P3.

know now several approximations that can be compared for working out common and variant features. A superposition on the CORE domains brings all ATP and AMP moieties to closely equivalent positions with mutual deviations below about 1 Å (data not shown). In the more local comparison given in Figure 8A, we superimposed only the phosphates 1, 2, and 5 common to all structures, but included in the figure *all* phosphates as well as side chains participating in the reaction.

First, Figure 8A reveals a dramatic positional variation of the fourth phosphate, demonstrating that all enzyme:Ap_5A complexes assume structures closer to the start of the forward reaction (ATP and AMP) than to the backward reaction (starting with ADP and ADP). Furthermore, the positional spread of the third phosphate is much larger than for the first, second, and fifth ones, indicating that this transferred phosphate is much looser than the others.

The positionally well-defined phosphates 1, 2, and 5 suffice for the construction of a trigonal bipyramid between oxygen atoms O23 and O45 of Ap_5A that circumscribes the transition state of the transferred phosphoryl group for the forward and the backward reaction (Müller-Dieckmann & Schulz, 1994). As can be visualized in Figure 8A, none of the "transferred" third phosphates and also not the "transferred" β-phosphate of the ADP at the NMP site of uridylate kinase are oriented exactly along the central line of this bipyramid. The average angular deviation of the O23···P3 bond is 14°. These deviations reflect the perturbations that are caused by the fourth phosphate in the Ap_5A complexes, by the imide bond in AMPPNP, and by the crystal contacts in the uridylate complex (Müller-Dieckmann & Schulz, 1994). We are dealing with smallish random changes that are likely to average out when comparing more structures, such that the natural arrangement emerges after extensive averaging. Here, we find that, although the average of the single deviations is 14°, the average of the O23···P3 vectors deviates by merely 7° from the central line.

Apart from the angular deviations of the "transferred" phosphate, we determined the length of the bipyramid, i.e., the O23···O45 distance, as 4.7 ± 0.2 Å, where the error is the RMS distance deviation among all structures depicted in Figure 8A. This length is the sum of the O23···P3 bond length of 1.6 Å and of 3.1 Å for the van der Waals distance between P3 and the attacking oxygen atom O45. This leaves no space for an in-line dissociative mechanism with a metaphosphate as the intermediate because this would require a O23···O45 distance of more than 6 Å.

The superposition of Figure 8A shows, furthermore, that the conserved residues Asp 89 (holding Mg^{2+} via two water molecules, see below Fig. 9) and Arg 132 (binding the third phosphate) are at rather conserved locations relative to phosphates 1, 2, and 5. A more peculiar situation is observed with the highly conserved fingerprint residue Lys 17 that assumes a number of different conformations in the evaluated structures, although it plays a major role in the phosphoryl transfer. The conformational spread points to plenty of allocated space. We therefore suggest that the ϵ-amino group of Lys 17 accompanies the transferred negative charge, which runs in the opposite direction of the phosphoryl transfer (from O45 to O23 in the forward reaction). Accounting for the rather large distance to the transferred phosphoryl group, it seems unlikely that the ϵ-amino group accompanies the third phosphate during transfer.

Among the known adenylate kinase structures, the Mg^{2+} required for the phosphoryl transfer has only been located in the reported Mg-structure. The Mg^{2+} position is also known in G-proteins, two of which were taken from the Brookhaven Protein Data Bank. In Figure 8B we superimposed the three equivalent phosphates of the high-resolution structure of H-ras-p21 (Pai et al., 1990) with those of the Mg-structure. This brought the Mg^{2+} ions to almost identical positions. The same is true for the other available G-protein structure (Noel et al., 1993; data not shown). Whereas the G-proteins have ideal octahedral Mg^{2+} ligand spheres (Fig. 8B), this does not apply for the adenylate kinases containing only a rather distorted half of an octahedron. Remarkably, the superposition of Figure 8B also brings the attacking water molecule-7 of the G-protein close to O45, the attacking oxygen in the adenylate kinases.

The Mg^{2+} environment of the adenylate kinases is depicted in further detail in Figure 9. The empty sixth ligand site and the lack of any peptide ligands like in the G-proteins (Pai et al., 1990; Noel et al., 1993; Coleman et al., 1994) conveys a rather dynamic picture. Most likely, Mg^{2+} accompanies the transferred phosphoryl group by moving along the indicated line versus OP5S. There is plenty of space for this motion and no hindrance from the two water molecules suspended by the highly conserved Asp 89 and by the third water ligand, which is merely

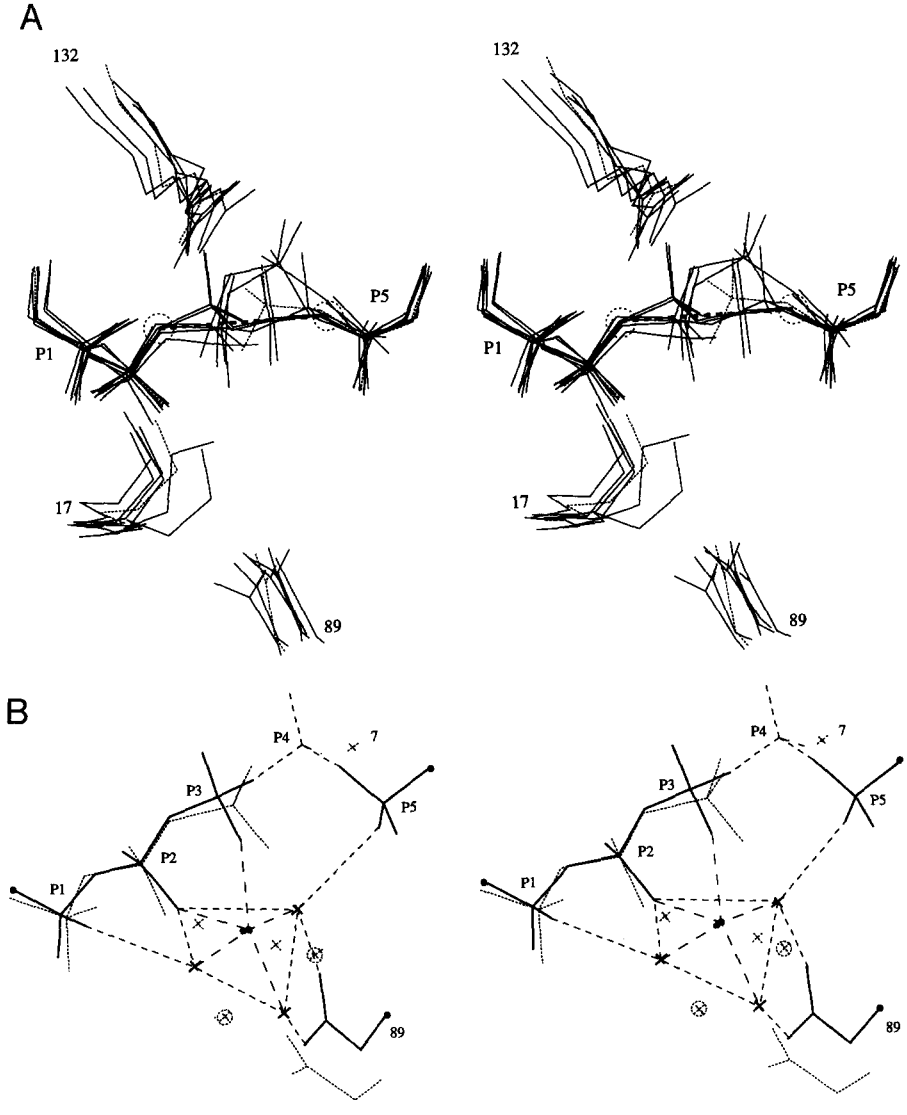

Fig. 8. Phosphate superpositions for the analysis of the phosphoryl transfer. **A:** Superposition of phosphates 1, 2, and 5 (or equivalents) for AK_{yst}:Ap_5A:Im, AK_{yst}:Ap_5A:Mg, AK_{eco}:Ap_5A (molecules I and II with molecule-I in two conformations; Müller & Schulz, 1992), AK_{eco}:AMPPNP:AMP (molecules 1 and 2; Berry et al., 1994), and uridylate kinase in complex with 2 ADP (dotted line; Müller-Dieckmann & Schulz, 1994). All other phosphates are depicted as well as the highly conserved residues Lys 17, Asp 89, and Arg 132. The connecting line (thick, dashed, ends encircled) between the average positions of O23 and O45 is the central line of the trigonal bipyramid circumscribing the transition state. **B:** Superposition of phosphates 1, 2, and 3 of AK_{yst}:Ap_5A:Mg with those of GMPPNP in H-ras-p21 (Pai et al., 1990). Mg^{2+} in the adenylate kinase is given as a black dot connected by dashed lines to its ligands. The additional fourth phosphate of Ap_5A is marked by dashed lines. All features of H-ras-p21 are depicted as dotted lines, including the attacking water molecule-7 and the two Mg^{2+} ligating water molecules (all crosses) as well as ligands Thr 61-O and Ser 40-O (crosses with circles, left to right). The Mg^{2+} ligand sphere in H-ras-p21 is a perfect octahedron.

held by a water network (Fig. 9). This gives a reasonable explanation for the forward reaction, which is approximated by all Ap_5A complexes (see above, Fig. 8A).

More difficult is the delineation of the backward reaction, because there is no appropriate water structure for holding Mg^{2+} at its expected position. Presumably, the starting structure for the backward reaction is less stable and therefore avoided in the Ap_5A complexes. Unfortunately, the uridylate kinase complex with two ADP molecules, which could be closer to the backward reaction structure, also fails to contain an appropriate water arrangement. It should be noted that, in this structure, the phosphate to be transferred in the backward reaction (β-phosphate of the ADP at the NMP-site) is not fully occupied and somewhat displaced (Müller-Dieckmann & Schulz, 1994), indicating also that this complex structure approximates the start of the forward reaction.

Materials and methods

Crystals

Two types of crystals were produced and analyzed, which eventually turned out to differ by a bound Mg^{2+} ion versus a bound Im molecule at the catalytic center. Initially, the Mg crystals were

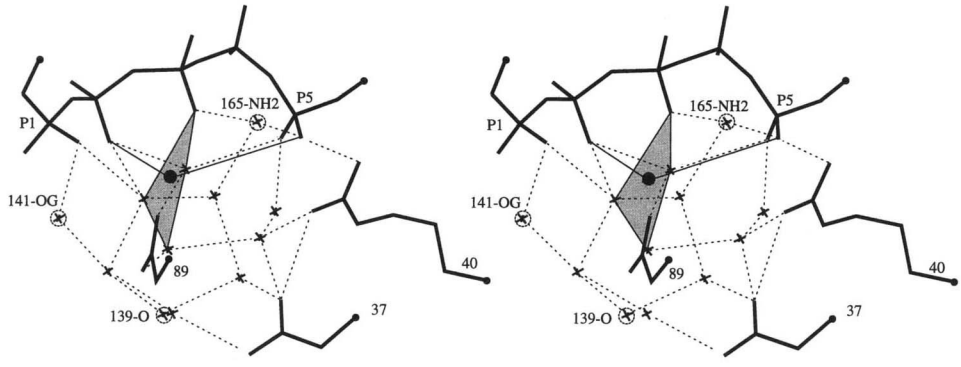

Fig. 9. Ligand sphere of Mg^{2+} in AK_{yst}:Ap_5A:Mg, which is formed by OP2S, OP3R, and water molecules 503, 505, and 506. The sphere forms half an octahedron with a hatched base plane; the apical ligand is OP2S (connected by a thin solid line). On transfer, the Mg^{2+} is likely to accompany the transferred third phosphate by moving along the inserted solid line toward OP5S, which in turn could be the apical ligand of a half octahedron for the back reaction starting with ADP and ADP. It should be remembered that among the depicted phosphates of Ap_5A, P1, P2, and P3 correspond to those of substrate ATP and P5 to AMP. P4 is the additional phosphate; it does *not* correspond to the second phosphate of ADP at the AMP site in the back reaction.

obtained with enzyme prepared from wet baker's yeast (Red Star, Universal Foods Co., Milwaukee, Wisconsin) according to Ito et al. (1980). The crystals were grown using hanging drops starting with 12 mg/mL protein, 1.1 mM Ap_5A, 26% PEG-8000 in 60 mM Im buffer at pH 7.2 in the drop and about 30% PEG-8000, 60 mM Im, pH 7.2, in the reservoir (Egner et al., 1987). The crystals were then transferred to a storage buffer containing 1.5 mM $MgCl_2$ in 26% PEG-8000, 100 mM NaCl, 1.2 mM Ap_5A, 1.0 mM NaN_3, 40 mM Tris-HCl at pH 7.2, where they remained for about 2 days.

Also the Im crystals were obtained from wet baker's yeast, but from a different supplier (Fala, Strasbourg). The purification procedure was that of Berger et al. (1989) up to the Cibacron-blue affinity column, which was then followed by hydroxylapatite chromatography and dialysis against 2.5 mM phosphate buffer (Muller, 1989). The crystallization conditions were the same as with the Mg crystals. The crystals invariably disintegrated, however, when being transferred to a Mg^{2+}-containing storage buffer. For X-ray analysis they were mounted directly from the mother liquor.

Presumably, the Ito et al. (1980) preparation procedure left some Mg^{2+} in the enzyme solution, which was incorporated in the Mg crystals, allowing them to survive 1.5 mM $MgCl_2$ in the storage buffer. In contrast, the other procedure with the final hydroxylapatite column had probably removed Mg^{2+} to such an extent that its site was occupied by an Im from the buffer. These crystals broke on exposure to Mg^{2+} because the Mg^{2+}–Im exchange affects crystal contacts (Tables 2, 3).

Both crystal forms contain Ap_5A and belong to space group P1. They are isomorphous but distinct from each other. The Im crystals have cell parameters $a = 36.3$ Å, $b = 40.5$ Å, $c = 45.7$ Å, $\alpha = 110.8°$, $\beta = 109.0°$, and $\gamma = 63.3°$ and diffract to a maximum resolution of about 1.5 Å. The cell parameter deviations of the Mg crystals are $\Delta a = -0.3$ Å (that means $a = 36.0$ Å), $\Delta b = -0.1$ Å, $\Delta c = -0.2$ Å, $\Delta\alpha = -0.1°$, $\Delta\beta = -0.2°$, and $\Delta\gamma = +1.4°$.

Data collection

The native data set of AK_{yst}:Ap_5A:Im was collected from four crystals with sizes of about 600 × 450 × 400 μm^3 using an area detector (model X1000; Xentronics/Siemens) with a rotating anode (model RU200B; Rigaku). Each data frame covered a 0.25° oscillation range measured within 3 min. X-ray intensities were processed with program XDS (Kabsch, 1988). The data collection yielded a total of 120,979 reflections with an upper resolution limit of 1.56 Å. Data processing reduced these to 25,713 unique reflections with $R_{sym} = \sum_{j,hkl} |I_{hkl}(j) - \langle I_{hkl}\rangle| / \sum_{j,hkl} I_{hkl}(j) = 6.6\%$. In order to restrict the analysis to high quality data, the resolution limit was lowered to 1.64 Å, resulting in 23,780 reflections with a completeness of 91%. This data set was used for the initial refinement. At a later stage, the area detector data (weight = 75%) were merged with 12,993 reflections in the range 2.0 to 1.63 Å (weight = 25%), measured on a diffractometer (model $P2_1$, Nicolet/Siemens). The difference between diffractometer and area detector data was $R_F = 2 \cdot \sum |F_1 - F_2| / \sum (F_1 + F_2) = 17.5\%$. The final data are specified in Table 1.

The native data set of AK_{yst}:Ap_5A:Mg is based on diffractometer data collected to 1.96 Å resolution from seven crystals. Furthermore, it contained diffractometer data collected by Egner (1986) out to 2.3 Å resolution. The final set is described in Table 1.

Structural refinement

Initially, the structure of the Mg crystals had been solved by multiple isomorphous replacement at 3 Å resolution and subjected to a preliminary refinement at 2.6 Å resolution that was stopped at an R-factor as high as 27.4% (Egner et al., 1987). The resulting model was essentially correct, but some loops in domain LID were grossly displaced. Using crystals from the same batch, the data collection was then extended to 1.96 Å resolution. Thereafter, we tried to include data from newly prepared crystals but experienced that these differed slightly but distinctly. A separate analysis of the new crystals revealed the bound Im.

As a consequence, we kept the data sets separate and refined the crystal forms AK_{yst}:Ap_5A:Mg and AK_{yst}:Ap_5A:Im independently from each other. In both refinements we used XPLOR (Brünger et al., 1987) with protocols similar to Stehle et al. (1991). At the end, the structure factors were modified by an overall anisotropic B-factor refinement, which in both struc-

tures reduced the *R*-factor by 0.9%. Incorporation of the new parameter files of Engh and Huber (1991) halved the RMS bond length and angle deviations (Table 1) but increased the *R*-factor by 0.2% in AK_{yst}:Ap_5A:Im, whereas the *R*-factor went unchanged in AK_{yst}:Ap_5A:Mg. The coordinates of the two reported structures are deposited in the Brookhaven Protein Data Bank.

Acknowledgments

We thank U. Egner and P.A. Karplus for part of the data collection and initial refinements, and A. Tomasselli as well as Y.A. Muller for supplying enzyme crystals. Coordinate supply by the Protein Data Bank, Brookhaven, New York, is appreciated.

References

Baker EN, Hubbard RE. 1984. Hydrogen bonding in globular proteins. *Prog Biophys Mol Biol 44*:97–179.

Berger A, Schiltz E, Schulz GE. 1989. Guanylate kinase from *Saccharomyces cerevisiae*. *Eur J Biochem 184*:433–443.

Berry MB, Meador B, Bilderback T, Liang P, Glaser M, Phillips GN Jr. 1994. The closed conformation of a highly flexible protein: The structure of *E. coli* adenylate kinase with bound AMP and AMPPNP. *Proteins Struct Funct Genet 19*:183–198.

Brünger AT, Kuriyan J, Karplus M. 1987. Crystallographic *R*-factor refinement by molecular dynamics. *Science 235*:458–460.

Coleman DE, Berghuis AM, Lee E, Linder ME, Gilman AG, Sprang SR. 1994. Structure of active conformations of $G_{i\alpha 1}$ and the mechanism of GTP hydrolysis. *Science 265*:1405–1412.

Diederichs K, Schulz GE. 1990. Three-dimensional structure of the complex between the mitochondrial matrix adenylate kinase and its substrate AMP. *Biochemistry 29*:8138–8144.

Diederichs K, Schulz GE. 1991. The refined structure of the complex between adenylate kinase from beef heart mitochondrial matrix and its substrate AMP at 1.85 Å resolution. *J Mol Biol 217*:541–549.

Dreusicke D, Karplus PA, Schulz GE. 1988. Refined structure of porcine cytosolic adenylate kinase at 2.1 Å resolution. *J Mol Biol 199*:359–371.

Dreusicke D, Schulz GE. 1986. The glycine-rich loop of adenylate kinase forms a giant anion hole. *FEBS Lett 208*:301–304.

Dunbrack RL Jr, Karplus M. 1993. Backbone-dependent rotamer library for proteins. Application to side-chain prediction. *J Mol Biol 230*:543–547.

Egner U. 1986. Röntgenstrukturanalyse eines Komplexes von der ATP:AMP Phosphotransferase aus Bäckerhefe und P^1,P^5-di(adenosin-5′-)pentaphosphat bei 0.26 nm Auflösung [dissertation]. Heidelberg: Universität Heidelberg.

Egner U, Tomasselli AG, Schulz GE. 1987. Structure of the complex of yeast adenylate kinase with the inhibitor Ap_5A at 2.6 Å resolution. *J Mol Biol 195*:649–658.

Engh RA, Huber R. 1991. Accurate bond and angle parameters for X-ray protein-structure refinement. *Acta Crystallogr A 47*:392–400.

Ito Y, Tomasselli AG, Noda LH. 1980. ATP:AMP phosphotransferase from baker's yeast: Purification and properties. *Eur J Biochem 105*:85–92.

Jones TA, Zou JY, Cowan SW, Kjeldgaard M. 1991. Improved methods for building protein models in electron density maps and the location of errors in these models. *Acta Crystallogr A 47*:110–119.

Kabsch W. 1988. Evaluation of single crystal X-ray diffraction from a position-sensitive detector. *J Appl Crystallogr 21*:916–924.

Karplus PA, Schulz GE. 1987. Refined structure of glutathione reductase at 1.54 Å resolution. *J Mol Biol 195*:701–729.

Kraulis PJ. 1991. MOLSCRIPT: A program to produce both detailed and schematic plots of protein structures. *J Appl Crystallogr 24*:946–950.

Luzzati V. 1952. Traitement statistique des erreurs dans la détermination des structures cristallines. *Acta Crystallogr 5*:802–810.

Magdolen V, Oechsner U, Bandlow W. 1987. The complete nucleotide sequence of the gene coding for adenylate kinase. *Curr Genet 12*:405–411.

Müller CW, Schulz GE. 1992. Structure of the complex between adenylate kinase from *E. coli* and the inhibitor Ap_5A refined at 1.9 Å resolution. *J Mol Biol 224*:159–177.

Müller CW, Schulz GE. 1993. Crystal structures of two mutants of adenylate kinase from *Escherichia coli* that modify the Gly-loop. *Proteins Struct Funct Genet 15*:42–49.

Müller-Dieckmann HJ, Schulz GE. 1994. The structure of uridylate kinase with its substrates: Geometry of the phosphoryl transfer transition state. *J Mol Biol 236*:361–367.

Muller YA. 1989. Röntgenstruktur-Untersuchungen an der Adenylatkinase aus Hefe und Versuche zur Kristallisation von Gewebe-Plasminogenaktivator [dissertation]. Freiburg im Breisgau, Germany: Universität Freiburg im Breisgau.

Noel JP, Hamm HE, Sigler PB. 1993. The 2.2 Å crystal structure of transducin-α complexed with GTPγS. *Nature (Lond) 366*:654–663.

Pai EF, Krengel U, Petsko GA, Goody RS, Kabsch W, Wittinghofer A. 1990. Refined structure of the triphosphate conformation of H-Ras p21 at 1.35 Å resolution: Implications for the mechanism of GTP hydrolysis. *EMBO J 9*:2351–2359.

Proba K, Tomasselli AG, Nielsen P, Schulz GE. 1987. The cDNA sequence encoding cytosolic adenylate kinase from baker's yeast (*Saccharomyces cerevisae*). *Nucleic Acids Res 15*:7187.

Read RJ. 1986. Improved Fourier coefficients for maps using phases from partial structures with errors. *Acta Crystallogr A 42*:140–149.

Reuner C, Hable M, Wilmans M, Kiefer E, Schiltz E, Schulz GE. 1988. Amino acid sequence and three-dimensional structure of cytosolic adenylate kinase from carp muscle. *Protein Sequences & Data Anal 1*:335–343.

Schulz GE. 1987. Structural and functional relationships in the adenylate kinase family. *Cold Spring Harbor Symp Quant Biol 52*:429–439.

Schulz GE. 1992. Binding of nucleotides by proteins. *Curr Opin Struct Biol 2*:61–67.

Schulz GE, Müller CW, Diederichs K. 1990. Induced-fit movements in adenylate kinases. *J Mol Biol 213*:627–630.

Stehle T, Ahmed SA, Claiborne A, Schulz GE. 1991. Structure of NADH peroxidase from *Streptococcus faecalis* 10C1 refined at 2.16 Å resolution. *J Mol Biol 221*:1325–1344.

Stehle T, Schulz GE. 1990. Three-dimensional structure of the complex of guanylate kinase from yeast with its substrate GMP. *J Mol Biol 211*:249–254.

Tomasselli AG, Mast E, Janes W, Schiltz E. 1986. The complete amino acid sequence of adenylate kinase from baker's yeast. *Eur J Biochem 155*:111–119.

Tsai MD, Yan HG. 1991. Mechanism of adenylate kinase: Site directed mutagenesis versus X-ray and NMR. *Biochemistry 30*:6806–6818.